

A Systematic Search for Changing-Look Quasars in SDSS

Chelsea L. MacLeod^{1*}, Nicholas P. Ross¹, Andy Lawrence¹, Mike Goad²,
Keith Horne³, William Burgett⁴, Ken C. Chambers⁵, Heather Flewelling⁵,
Klaus Hodapp⁵, Nick Kaiser⁵, Eugene Magnier⁵, Richard Wainscoat⁵,
Christopher Waters⁵

¹*Institute for Astronomy, University of Edinburgh, Royal Observatory, Edinburgh, EH9 3HJ, U. K.*

²*Department of Physics and Astronomy, University of Leicester, University Road, Leicester, LE1 7RH, U. K.*

³*SUPA Physics & Astronomy, North Haugh, St Andrews KY16 9SS, U. K.*

⁴*GMTO Corp., 251 S. Lake Ave., Pasadena, CA 91101 USA*

⁵*Institute for Astronomy, University of Hawaii, 2680 Woodlawn Dr., Honolulu, HI 96822, USA*

Accepted XXX. Received YYY; in original form ZZZ

ABSTRACT

We present a systematic search for changing-look quasars based on repeat photometry from SDSS and Pan-STARRS1, along with repeat spectra from SDSS and SDSS-III BOSS. Objects with large, $|\Delta g| > 1$ mag photometric variations in their light curves are selected as candidates to look for changes in broad emission line (BEL) features. Out of a sample of 1011 objects that satisfy our selection criteria and have more than one epoch of spectroscopy, we find 10 examples of quasars that have variable and/or “changing-look” BEL features. Four of our objects have emerging BELs; five have disappearing BELs, and one object shows tentative evidence for having both emerging *and* disappearing BELs. With redshifts in the range $0.20 < z < 0.63$, this sample includes the highest-redshift changing-look quasars discovered to date. We highlight the quasar J102152.34+464515.6 at $z = 0.204$. Here, not only have the Balmer emission lines strongly diminished in prominence, including $H\beta$ all but disappearing, but the blue continuum $f_\nu \propto \nu^{1/3}$ typical of an AGN is also significantly diminished in the second epoch of spectroscopy. Using our selection criteria, we estimate that $> 15\%$ of strongly variable luminous quasars display changing-look BEL features on rest-frame timescales of 8 to 10 years. Plausible timescales for variable dust extinction are factors of 2–10 too long to explain the dimming and brightening in these sources, and simple dust reddening models cannot reproduce the BEL changes. On the other hand, an advancement such as disk reprocessing is needed if the observed variations are due to accretion rate changes.

Key words: (galaxies:) quasars: emission lines < Galaxies – (galaxies:) quasars: general < Galaxies – galaxies: active < Galaxies – accretion, accretion discs < Physical Data and Processes

1 INTRODUCTION

Due to modern photometric, spectroscopic, and time-domain sky surveys, we are now able to distinguish between the ubiquitous properties of quasars and rare, discrepant behavior, suggestive of new physics. The continuum variability of a quasar¹ is typically 0.2 mag on timescales of \sim months to years and has been well-characterized for large quasar samples using the Sloan Digital Sky Survey

(SDSS; e.g., Vanden Berk et al. 2004; Wilhite et al. 2005; Sesar et al. 2007; Schmidt et al. 2010; Butler & Bloom 2011; MacLeod et al. 2012) and more recently Pan-STARRS1 (PS1; Morganson et al. 2014, 2015; Simm et al. 2015). A common interpretation of this variability involves localized accretion disk instabilities, but the precise mechanisms are still under debate (e.g., Dexter & Agol 2011; Kelly et al. 2011; Kokubo 2015, and references therein). For example, the color dependence and near simultaneity of variability pose severe problems (see Lawrence 2012, and references therein). In Seyfert galaxies, time lags of hours to days suggest that the optical continuum variability is driven at least in part by reprocessing of EUV or X-ray light (e.g.,

* email: cmacleod@roe.ac.uk

¹ We use the term quasar to mean a bolometrically luminous, $\gtrsim 10^{46}$ erg s⁻¹, active galactic nucleus (AGN).

Collier et al. 1998; Sergeev et al. 2005; Cackett et al. 2007; Shappee et al. 2014; Edelson et al. 2015) but this may be due to inner cloud reprocessing rather than the disc itself (Lawrence 2012), and the reliability of the interband lags has been questioned (Korista & Goad 2001; Gaskell 2007).

While the UV/optical continuum varies ubiquitously among quasars, typically in a ‘bluer-when-brighter’ fashion (e.g., Wilhite et al. 2005; Schmidt et al. 2012; Ruan et al. 2014), the broad emission lines (BELs) seen in quasar spectra are usually less variable and lagged with respect to the continuum, as seen in reverberation mapping studies (e.g., Clavel et al. 1991; Peterson 1993; Grier et al. 2012; Peterson 2014; Shen et al. 2015). Results from such studies indicate that the BELs are formed by photoionization by continuum photons, and that the broad line region (BLR) spans a range in density, ionization state, and distance from the central black hole, which is typically $R/c \approx 0.1d(L/10^{46} \text{ erg s}^{-1})^{1/2}$. Some BELs show a Baldwin effect, where the line equivalent width (EW) decreases with increasing continuum luminosity (Baldwin et al. 1978; Kinney et al. 1990). In general, it seems that the underlying spectral energy distribution (SED) influences the wind structure and the high-ionization BEL parameters (Richards et al. 2011). Because $H\beta$ in particular, and to some extent MgII basically count the number of ionizing photons and are less sensitive to changes in the AGN SED than the high ionization lines, neither line shows a particularly strong global Baldwin effect (Dietrich et al. 2002). However, an intrinsic Baldwin effect is seen and expected in an individual source (for $H\beta$ see Gilbert & Peterson 2003; Goad et al. 2004; Cackett & Horne 2006). Furthermore, BELs may respond differently to changes in ionizing continuum flux if the average formation radius is different. For example, Goad et al. (1993) and O’Brien et al. (1995) show that MgII responds less to continuum changes relative to the other BELs (e.g., $H\beta$) due to its larger average formation radius and weak intrinsic response.

Emerging or disappearing BELs have been discovered in several relatively local AGN (Khachikian & Weedman 1971; Tohline & Osterbrock 1976; Penston & Perez 1984; Cohen et al. 1986; Bischoff & Kollatschny 1999; Aretxaga et al. 1999; Eracleous & Halpern 2001; Shappee et al. 2014; Denney et al. 2014; Li et al. 2015), and recently in a higher-redshift $z = 0.3$ quasar SDSS J015957.64+003310.4 (hereafter, J0159+0033; LaMassa et al. 2015). These BEL changes are often associated with large, factor $\gtrsim 10$ changes in the continuum flux; the two are probably linked to the same physical mechanism, as such BEL and continuum changes are rare in AGN. This “changing-look” behavior is valuable for understanding the structure of the accretion disk and BLR. One possible physical scenario that could explain this behavior is variable obscuration by dust or gas clouds passing across the line of sight (e.g., Goodrich 1989; Tran et al. 1992; Risaliti et al. 2009). While strong arguments exist for variable absorption of the X-ray emitting region in some AGN (Risaliti et al. 2009), it is relatively difficult to explain variable obscuration of the much larger UV/continuum region, as it is unclear what population of clouds would exist at sufficiently large radii (e.g., Nenkova et al. 2008a,b). Indeed, a simple change in extinction fails to explain the observations of J0159+0033 (LaMassa et al. 2015). Instead,

the transition might be due to a change in available ionizing flux from the central engine. LaMassa et al. (2015) suggest that such a change would be consistent with the disk-wind scenario of Elitzur et al. (2014), where a decrease in the accretion rate, and consequently the level of ionizing flux, would cause the BELs to disappear as the system evolves from Type 1 to 1.2/1.5 to 1.8/1.9². An alternative scenario was proposed by Merloni et al. (2015) in which J0159+0033 underwent a flaring episode due to a tidal disruption event of a star by the supermassive black hole.

Motivated by the discovery of a single changing-look quasar in SDSS by LaMassa et al. (2015), in this paper we undertake a systematic search for similar objects with candidate ‘changing-look’ quasars being selected from their light curves over the course of SDSS and PS1. Our search is sensitive to emerging or disappearing BELs that may be associated with strong increases or decreases in flux in quasars which were more luminous than $M_i = -22.0$ with $i > 15.0$ roughly ten years ago. In particular, what is being observed and reported here is the (dis)appearance of broad Balmer emission lines, and a strengthening (weakening) of MgII emission.

The outline of the paper is as follows. In Section 2, we describe the SDSS and PS1 data used in this study. In Section 3, we describe the sample selection. We present the results from our search in Section 4, describing a set of 10 quasars, five of which have disappearing BELs, four of which have appearing BELs, and one object that potentially has evidence for both disappearing and appearing BEL behavior. In Section 5, we discuss the timescales associated with the changing-look BEL phenomenon, and calculate probabilities of observing the quasar BEL changes as a function of (rest-frame) timescale. We conclude in Section 6. All photometric measurements are normalized to the AB-magnitude system. Where needed, we adopt a flat Λ CDM cosmology with $H_0 = 70 \text{ km s}^{-1} \text{ Mpc}^{-1}$ and $\Omega_m = 0.30$.

2 DATA

For our search of candidate changing-look quasars, we utilize three imaging data sets as well as spectroscopy from the SDSS-I/II and SDSS-III surveys.

2.1 Imaging Data

We use imaging data from the SDSS, SDSS-III, PS1 and Catalina Sky Survey. As a guide to the baseline of the observations, SDSS started its imaging campaign in 2000 and concluded in 2007, having covered 11,663 deg². These data are part of the SDSS-I/II survey and are described in Abazajian et al. (2009) and references therein. SDSS-III added another ~ 3000 deg² of new imaging area in 2008. Pan-STARRS imaging commenced in 2009 and continued through to 2013. Hence, the addition of the PS1 photometry to the SDSS photometry increases the baseline of observations from ≈ 8 to ≈ 14 years.

² We follow the classical definitions of optical types, where the total flux in $H\beta$ relative to [OIII] decreases going from type 1.2 to 1.8, and type 1.9 is defined as having broad $H\alpha$ but lacking any broad $H\beta$ (Osterbrock 1981).

2.1.1 SDSS

The SDSS (York et al. 2000) uses the imaging data gathered by a dedicated 2.5m wide-field telescope (Gunn et al. 2006), which collected light from a camera with 30 2k×2k CCDs (Gunn et al. 1998) over five broad bands - *ugriz* (Fukugita et al. 1996) - in order to image 14,555 unique deg² of the sky. This area includes 7,500 deg² in the North Galactic Cap (NGC) and 3,100 deg² in the South Galactic Cap (SGC). The imaging data are taken on dark photometric nights of good seeing (Hogg et al. 2001) and are calibrated photometrically (Smith et al. 2002; Ivezić et al. 2004a; Tucker et al. 2006; Padmanabhan et al. 2008), and astrometrically (Pier et al. 2003) before object parameters are measured (Lupton et al. 2001; Stoughton et al. 2002). The Eighth Data Release (DR8; Aihara et al. 2011) provides updated photometric calibrations.

The Stripe 82 region of SDSS (S82; 22h 24m < R.A. < 04h 08m and |Dec.| < 1.27 deg) covers ~300 deg² and has been observed ~60 times on average to search for transient and variable objects (Abazajian et al. 2009). These multi-epoch data have time scales ranging from 3 hours to 8 years and provide well-sampled 5-band light curves for an unprecedented number of quasars (see Sesar et al. 2007; Schmidt et al. 2010; Ai et al. 2010; MacLeod et al. 2010; Meusinger et al. 2011; Butler & Bloom 2011, for examples of quasar variability studies based on S82 photometry).

In addition to the DR8 photometry provided on the SDSS website, our analysis utilizes the S82 database of quasars in MacLeod et al. (2012), which includes observations taken in nonphotometric conditions and recalibrated using the improved method of Ivezić et al. (2004b). While the latter dataset only includes point sources, we consider both resolved and unresolved observations from DR8, adopting PSF magnitudes in each case³. We define a source to be in S82 if it is in the S82 database of MacLeod et al. (2012) or in the (R.A., Dec.) range defined above.

2.1.2 Pan-STARRS1 3 π Survey

Our analysis includes imaging from the PS1 3 π survey (Kaiser et al. 2002), in particular the Processing Version 2 catalog available in a local DVO database (released January 2015). PS1 comprises a 1.8m telescope equipped with a 1.4-gigapixel camera. Over the course of 3.5 years of the 3 π survey, up to four exposures per year in 5 bands, $g_{P1}, r_{P1}, i_{P1}, z_{P1}, y_{P1}$ have been taken across the full $\delta > -30^\circ$ sky (for full details, see Tonry et al. 2012; Metcalfe et al. 2013). Each nightly observation consists of a pair of exposures 15 min apart to search for moving objects. For each exposure, the PS1 3 π survey has a typical 5 σ depth of 22.0 in the *g*-band (Inserra et al. 2013). The overall system, photometric system, and the PS1 surveys are

³ We adopt PSF magnitudes throughout our analysis, although ideally CMODEL (KRON) magnitudes should be used for extended sources in SDSS (PS1). Since we are only interested in large magnitude changes in the central regions of any object, the differences in magnitude types should not appreciably affect our results. Also, we do not correct the magnitudes for Galactic absorption, as we are only interested in magnitude differences.

described in Kaiser et al. (2010), Stubbs et al. (2010), and Magnier et al. (2013), respectively.

2.1.3 Catalina Sky Survey

While not included in our analysis, where instructive, we also show data from the Catalina Sky Survey second release (CRTS; Drake et al. 2009). The CRTS magnitudes are based on unfiltered light but calibrated to a *V*-band zero-point. We average the CRTS data in segments of 10 days for visual clarity, and apply a constant offset m_0 so that the data match any simultaneous SDSS *g*-band observations.

2.2 Spectroscopic Data

We use the spectroscopic observations of quasars that are given in the SDSS Data Release Seven catalog (DR7Q) from Schneider et al. (2010).

As described by Richards et al. (2002), quasar target candidates are selected for spectroscopic observations based on their optical colors and magnitudes in the SDSS imaging data or their detection in the FIRST radio survey (Becker et al. 1995). Low-redshift, $z \lesssim 3$, quasar targets are selected based on their location in *ugri*-color space and the quasar candidates passing the *ugri*-color selection are selected to a flux limit of $i = 19.1$. High-redshift, $z \gtrsim 3$, objects are selected in *griz*-color space and are targeted to $i = 20.2$. Furthermore, if an unresolved, $i \leq 19.1$ SDSS object is matched to within 2" of a source in the FIRST catalog, it is included in the quasar selection.

The final quasar catalog from SDSS-I/II, based on the Seventh Data Release of SDSS (DR7; Abazajian et al. 2009), is presented in Schneider et al. (2010). This catalog contains 105,783 spectroscopically confirmed quasars that have luminosities larger than $M_i = -22.0$.

In order to look for significant changes in the BELs, we require (at least) a second epoch of spectroscopy. This is supplied by the Baryon Oscillation Spectroscopic Survey (BOSS; Dawson et al. 2013) which was part of the third incarnation of the SDSS (SDSS-III; Eisenstein et al. 2011).

We apply no selection to the type of BOSS spectroscopic target that is utilised for the later epoch of spectroscopy; i.e., a DR7 SDSS quasar that is a “changing-look” candidate can be classified as a BOSS galaxy. Indeed, of the final sample of 10 objects presented in this work, only 3 are actually in the SDSS-III BOSS DR12 Quasar Catalog of Pâris et al. (2016, in advanced prep.). We give further details of the repeat spectroscopic targeting in the Appendix.

The BOSS spectrographs and their SDSS predecessors are described in detail by Smee et al. (2013). In brief, there are two double-armed spectrographs that are significantly upgraded from those used by SDSS-I/II. Exposed to a minimum signal-to-noise ratio of $\sqrt{10}$ in *g* and $\sqrt{20}$ in *i* (~1.6 hr/plate; Dawson et al. 2013), they cover the wavelength range 3600 Å to 10,400 Å with a resolving power of 1500 to 2600 (Smee et al. 2013). In addition, the throughputs have been increased with new CCDs, gratings, and improved optical elements, and the 640-fibre cartridges with 3" apertures have been replaced with 1000-fibre cartridges with 2" apertures. Ultimately, the throughput of the BOSS spectrographs are considerably greater (in the red and the

blue), and span a greater wavelength range, than the original SDSS instruments.

The BOSS spectra presented in this work all have LAMBDA_EFF=5400Å (Dawson et al. 2013), i.e., the SDSS plate holes were drilled to maximize the signal-to-noise at 5400Å, and therefore do not need the spectrophotometric corrections from Margala et al. (2015). Also, the BOSS spectra presented here do not have the PROGRAM=APBIAS target flag, which would indicate an offset in the fiber position with respect to the earlier SDSS spectrum.

2.3 Multi-wavelength Coverage

We cross-matched our superset of quasars with various radio and X-ray catalogs. We use the combined radio catalog of Kimball & Ivezić (2014), which includes sources from five radio catalogs (FIRST, NVSS, GB6, WENSS, and VLSSr), to help identify blazar contaminants in S82 during the selection process. We check the latest release of the XMM-Newton serendipitous source catalog (Rosen et al. 2015) and the Chandra Source Catalog (CSC; Evans et al. 2010) for archival X-ray observations of any interesting objects from our search.

3 SAMPLE SELECTION

Our superset is any object listed in the DR7Q catalog of spectroscopically confirmed quasars, which includes both point-sources and resolved objects with $M_i < -22$. To select quasars that may have varying spectral features, we quantify the photometric properties of this spectroscopic quasar dataset and assume that significant BEL changes will be associated with a significant change in flux. We use the g -band SDSS photometry and extend the time baseline from 10 to 15 years by including g -band PS1 photometry in our analysis⁴. Since our aim is to find changing-look quasars, we search for quasars that, along with the earlier spectrum in SDSS DR7, have a later spectrum in BOSS.

Initially, we limit our sample to the S82 region, so that a well-sampled light curve exists for each object, making it easier to identify true large-amplitude photometric variability. There are 9474 quasars in S82, including extended sources which are not in the point source catalog of MacLeod et al. (2012). Motivated by the light curve for J0159+0033, we search for quasars that show at least a 1.0 mag dimming or brightening in the g -band among any observations in the combined SDSS and PS1 light curve⁵. For objects with at least ten photometric data points, light curve outliers are flagged as being 0.5 mag away in g from the light curve running median ($\sim 30\%$ of the sample). Since our aim is to find large, gradual changes in flux without a significant

⁴ The SDSS g filter is close enough to the g_{P1} filter in overall response that we can ignore any color terms.

⁵ For a similar search but for large-amplitude (1.5 mag) nuclear brightening in resolved SDSS galaxies, see Lawrence et al. (2012), which utilizes results from the PS1 Faint Galaxy Supernova Survey available at <http://star.pst.qub.ac.uk/sne/ps1fgss/psdb/>.

Selection	Total #	In S82
SDSS Quasars in DR7Q	105783	9474
with BOSS spectra	25484	2304
and $ \Delta g > 1$ mag and $\sigma_g < 0.15$ mag	1011	287
and that show variable BELs	10	7

Table 1. Selection of spectroscopically variable quasars.

amount of contamination due to poor photometry, we reject these light curve outliers during the variability selection. This selects 1692 objects with $|\Delta g| > 1$ mag and photometric uncertainties $\sigma_g < 0.15$ mag. Approximately 15% of these were observed again with the BOSS spectrograph; we focus on these 287 objects. Thirty-six objects in this subsample are detected in the radio, and of these, three were clearly blazars, as they were radio sources and exhibited fast and large-amplitude variability (2–3 mag within months; e.g. Ruan et al. 2012). We do not consider these three objects in our further analysis, as we are interested in BEL changes unrelated to blazar activity. After visually searching through all SDSS/BOSS spectra for BELs that are clearly present in one epoch but not another, we identify seven quasars from S82 in which at least some BELs satisfy this criterion.

We then extend our search to the entire SDSS footprint, which contains 105783 quasars in DR7Q. Of the 105746 quasars ($> 99\%$) which have PS1 detections, 6348 have shown at least a 1.0 mag change in their g -band light curves. Of these, 1011 have BOSS spectra, which includes the 287 quasars from S82. After visually inspecting each spectrum, we find three additional quasars with disappearing BELs. The final yield is higher for the S82 sample due to the improved cadence; we are able to more efficiently identify high-amplitude variability as well as more reliably identify spurious data points⁶. The distributions of the time scales and magnitude changes involved are shown in Fig. 1. This selection algorithm skews our search to those objects showing BEL changes over roughly ten years, since this is the timespan between SDSS and BOSS spectra, although the rest-frame timescales probe down to shorter timescales (bottom panel). The improved time coverage of the S82 regions can also be seen from the contours in the panels; the S82 sample (in white) fills in gaps in $|\Delta t|$ while reaching to larger $|\Delta g|$.

Our sample selection is given in Table 1.

4 THE CHANGING-LOOK QUASARS

Our initial search through the S82 quasars yielded the following results: (i) significant BEL changes are seen on long timescales (~ 2000 to 3000 days in the rest frame) in the selected sample; (ii) these changes are associated with large ($|\Delta g| \sim 1$) amplitude changes in the photometry, and (iii) emerging (disappearing) BEL features correspond to continuum brightening (dimming). Given the extra temporal

⁶ Without having a well-sampled light curve, outliers due to poor photometry are more difficult to identify by our algorithm and therefore can cause the object to pass the $|\Delta g| > 1$ mag criterion.

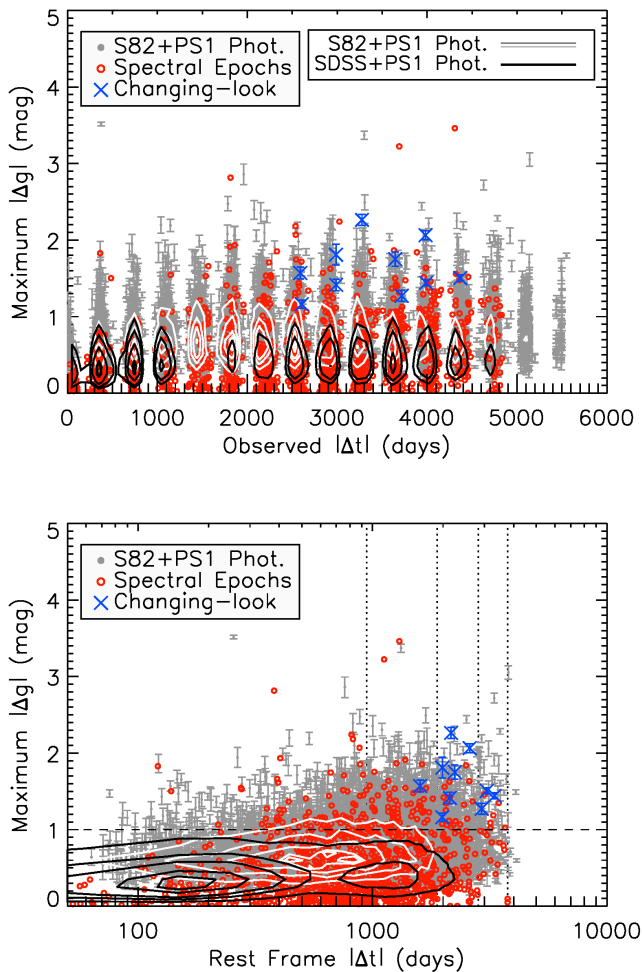


Figure 1. Distribution of the maximum magnitude difference $|\Delta g|_{\max}$ versus time lag $|\Delta t|$. The black contours show the distribution for the superset of quasars (DR7Q), which is based on SDSS and PS1 photometry. The white contours are the same but for the subsample of quasars in S82, which are shown as grey data points (one point per S82 quasar). The contours show regions containing 5, 10, 25, 50, and 75% of the data. The subsample of DR7Q with repeat spectra and $|\Delta g| > 1$ photometric changes are shown by open red circles, but now showing the $|\Delta g|_{\max}$ spanned by the *spectroscopic* epochs versus the corresponding time between spectra. For objects with multiple spectra, we choose the two epochs spanning the largest $|\Delta g|$ for display here. While the data are clumped into “seasons” in the top panel, the distribution is smoothed out when switching to rest-frame time lag in the bottom panel. Our final selection is limited to quasars with repeat spectra with $|\Delta g|_{\max} > 1$ (indicated by the horizontal dashed line). The final sample of 10 objects are plotted as blue crosses.

information provided by S82 light curves, our selection algorithm could more easily identify large-amplitude outbursts and reliably reject spurious data points, yielding seven objects of interest in S82.

When extended to the full SDSS footprint, where the inclusion of the PS1 3π photometry generated lightcurves for $>99\%$ of the DR7Q quasars, our combined search yielded three additional objects (Table 1). We present all 10 objects

here: four that show *appearing* BEL features, five that show *disappearing* BELs⁷, and one that shows evidence for both.

Our final sample of changing-look quasars is listed in Table 2, and the redshift distribution is compared to the full quasar sample in Fig. 2. We note that all of our objects are at $z < 0.63$, but this is potentially a selection effect, as we discuss in Section 5. However, this sample extends the range of known changing-look AGN to $z = 0.63$ at quasar luminosities. In Fig. 3, the 5007\AA [O III] luminosity is shown as a function of redshift for the full DR7Q sample and our final objects. Examples of previously studied changing-look AGN are also shown for comparison. The [O III] luminosity is often used as a proxy of the intrinsic AGN luminosity (e.g., Kauffmann et al. 2003; Heckman et al. 2004), so that Fig. 3 is a comparison of the intrinsic brightness and redshift of changing-look AGN.

In the following sections, we compute the flux deviation between two spectra at any given wavelength, $N_\sigma(\lambda) = (f_2 - f_1) / \sqrt{\sigma_2^2 + \sigma_1^2}$ (e.g., Filiz Ak et al. 2012), to determine the significance (in units of σ per spectral pixel) of a BEL change. In particular, we assess the significance of a BEL change by comparing its flux deviation to that of the underlying continuum at that wavelength. Note that the significance of BEL changes will be higher than that quoted here when $N_\sigma(\lambda)$ is integrated over the pixels spanning the BEL. In the few cases where there are more than two spectra available, we adopt the two spectra with the largest time lag unless otherwise stated.

In each case, the difference spectrum $|\Delta f_\lambda| = |f_{\text{BOSS}} - f_{\text{SDSS}}|$ is presented. $|\Delta f_\lambda|$ is fit as a power-law after masking out the H α , H β , H δ , H γ , Mg II and He I BELs and allowing the normalization to vary. The best-fit power-law indices β are listed in Table 2 and are based on the spectra listed in the preceding columns. We compare the best fits to a $f_\nu \propto \nu^{1/3}$ power law since this form is expected if the variable component resembles a standard thin disk (Shakura & Sunyaev 1973).

4.1 Appearing BELs

Four objects that show evidence of appearing BELs are plotted in Fig. 4. In all cases, the flux increased dramatically ($|\Delta g| > 1$ mag). The light curves in the top two panels of Fig. 4 show a “flat-topped” behavior, i.e., rising over ~ 1000 days in the observed frame to a constant luminosity. J214613.31+000930.8 (second panel) is the only object from our final sample that has a radio detection. In all cases, H β is absent from the first spectrum while Mg II is observed at low signal-to-noise. In general, however, the significance for appearing BELs in our sample is not very high ($\lesssim 3\sigma$ per spectral pixel for all H β transitions) for two reasons. First, in order to be included in our search, the source must be a BEL quasar in the initial DR7 spectrum, thus making any further BEL brightening less significant. Second, the improved BOSS spectrograph provides higher quality spectra

⁷ One object, SDSS J214822.25+011217.6, is not considered part of our sample although it exhibited a disappearing BEL; the disappearance was due to the appearance of a broad absorption line, which is a different phenomenon than the changing-look behavior studied here (see Filiz Ak et al. 2012).

Table 2. SDSS Quasars with emerging or disappearing BELs. Δg is the largest magnitude change observed, and Δt_{RF} is the time span for this change in the rest frame of the quasar. J015957.64+003310.4 is the (first) changing-look quasar discovered by [LaMassa et al. \(2015\)](#). $\text{Max}(\Delta g)$ is defined such that positive values imply a dimming in the light curve. The last column lists the best-fit power-law index β for the difference spectrum.

Name (SDSS J)	z	$\text{Max}(\Delta g)$	Δt_{RF} (days)	BEL behavior	(MJD plate fiber) ₁	(MJD plate fiber) ₂	$ \Delta f_{\nu} \propto \nu^{\beta}$
002311.06+003517.5	0.422	-1.50 ± 0.04	3072	Appear	51816 0390 0564	55480 4219 0852	0.04 ± 0.02
015957.64+003310.4	0.312	1.16 ± 0.06	1985	Disappear	51871 0403 0549	55201 3609 0524	0.27 ± 0.02
022556.07+003026.7	0.504	1.81 ± 0.14	1985	Both	52944 1508 0556	55445 3615 0617	0.16 ± 0.03
022652.24-003916.5	0.625	1.75 ± 0.09	2242	Disappear	52641 1071 0281	56577 6780 0339	0.2 ± 0.1
100220.17+450927.3	0.400	1.41 ± 0.07	2134	Disappear	52376 0943 0310	56683 7284 0122	-0.20 ± 0.02
102152.34+464515.6	0.204	1.44 ± 0.04	3313	Disappear	52614 0944 0603	56769 7386 0410	0.175 ± 0.007
132457.29+480241.2	0.272	1.27 ± 0.07	2923	Disappear	52759 1282 0045	56805 7406 0527	0.86 ± 0.02
214613.31+000930.8	0.621	-1.57 ± 0.08	1597	Appear	52968 1107 0358	55478 4196 0774	0.1 ± 0.1
225240.37+010958.7	0.534	-2.06 ± 0.06	2596	Appear	52174 0676 0442	55500 4294 0045	-0.45 ± 0.08
233317.38-002303.4	0.513	-2.26 ± 0.07	2164	Appear	52199 0681 0114	55447 4212 0312	0.75 ± 0.07

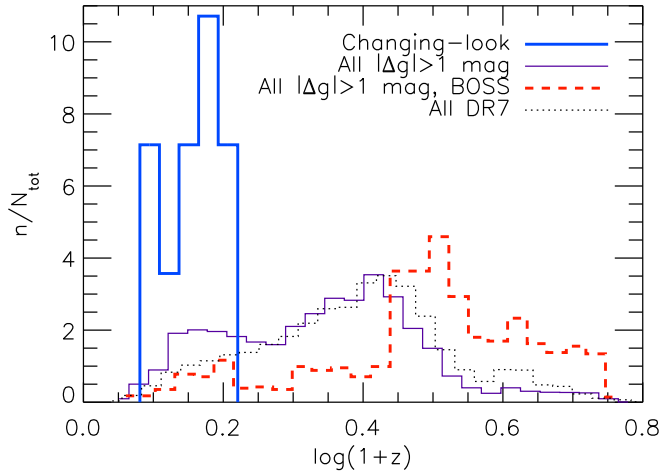


Figure 2. Normalized redshift distributions for the sample of changing-look quasars (in blue), the full sample of $N_{\text{tot}} = 6348$ highly variable quasars (purple), the subset with BOSS spectra (dashed red; $N_{\text{tot}} = 1011$), and the entire DR7 quasar catalog (dotted; $N_{\text{tot}} = 105,783$). n indicates the number of points in a bin divided by the bin width, and each histogram has unit area.

than the SDSS spectrograph, so if the source is faint in the earlier spectroscopic epoch, its spectrum will be correspondingly relatively noisy. However, with these caveats in mind, it is notable that our search produced a similar number of appearing and disappearing BEL cases.

4.2 Disappearing BELs

The five objects that show evidence of disappearing BELs are plotted in Fig. 5. In all cases, the g -band flux dropped significantly from the SDSS spectroscopic epoch to the BOSS epoch.

We recover J0159+0033 in our search (top panel of Fig. 5), which shows a vanishing $H\beta$ at 4σ significance. Among our 10 final objects, this is the only one present in the XMM or *Chandra* catalog. J022652.24–003916.5, shown

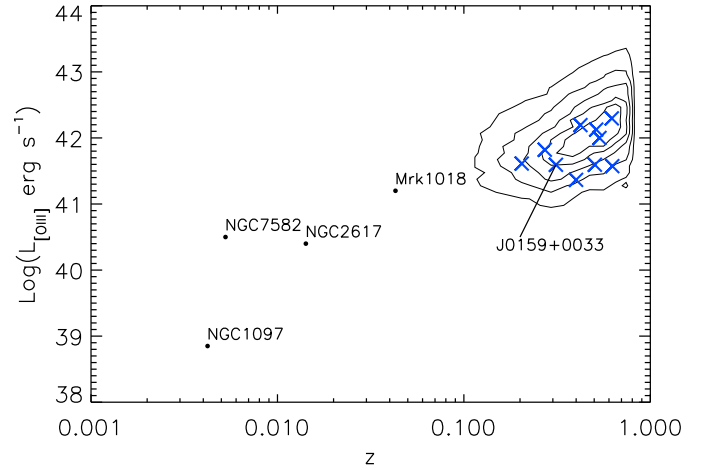


Figure 3. $[\text{O III}]$ luminosity versus redshift for the DR7Q sample (contours), our final sample of 10 (blue crosses), and examples of previously known changing-look AGN (black points; cf. Fig. 1 in [LaMassa et al. 2015](#)). For the DR7Q sample, we adopt values from [Shen et al. \(2011\)](#).

in the second panel, showed a similar behavior, and multiple BOSS spectra reveal the object in an intermediate phase between MJD ≈ 55200 and 56250 (cyan and purple spectra). In this case, the Mg II BEL is barely present. However, the BEL disappearance in this object is at low significance ($< 2\sigma$) since the source is faint ($20.5 < g < 22$). The remaining panels show three objects from outside S82 where $H\beta$ vanishes at $> 3\sigma$ significance. The object J102152.34+464515.6 (hereafter J1021+4645), shown in the third panel, demonstrates a highly significant (8σ) change from a Type 1.0 to a Type 1.9 AGN, and we elaborate on this object in Section 5. In the dim-state spectrum for SDSS J100220.17+450927.3, the broad Mg II line is still present, but the $H\beta$ line is absent.

The BOSS spectrum for J132457.29+480241.2, shown in the last panel, was unrecoverable redward of $H\beta$ due to data extraction issues associated with that particular BOSS fiber. However, an additional spectrum was obtained in Jan-

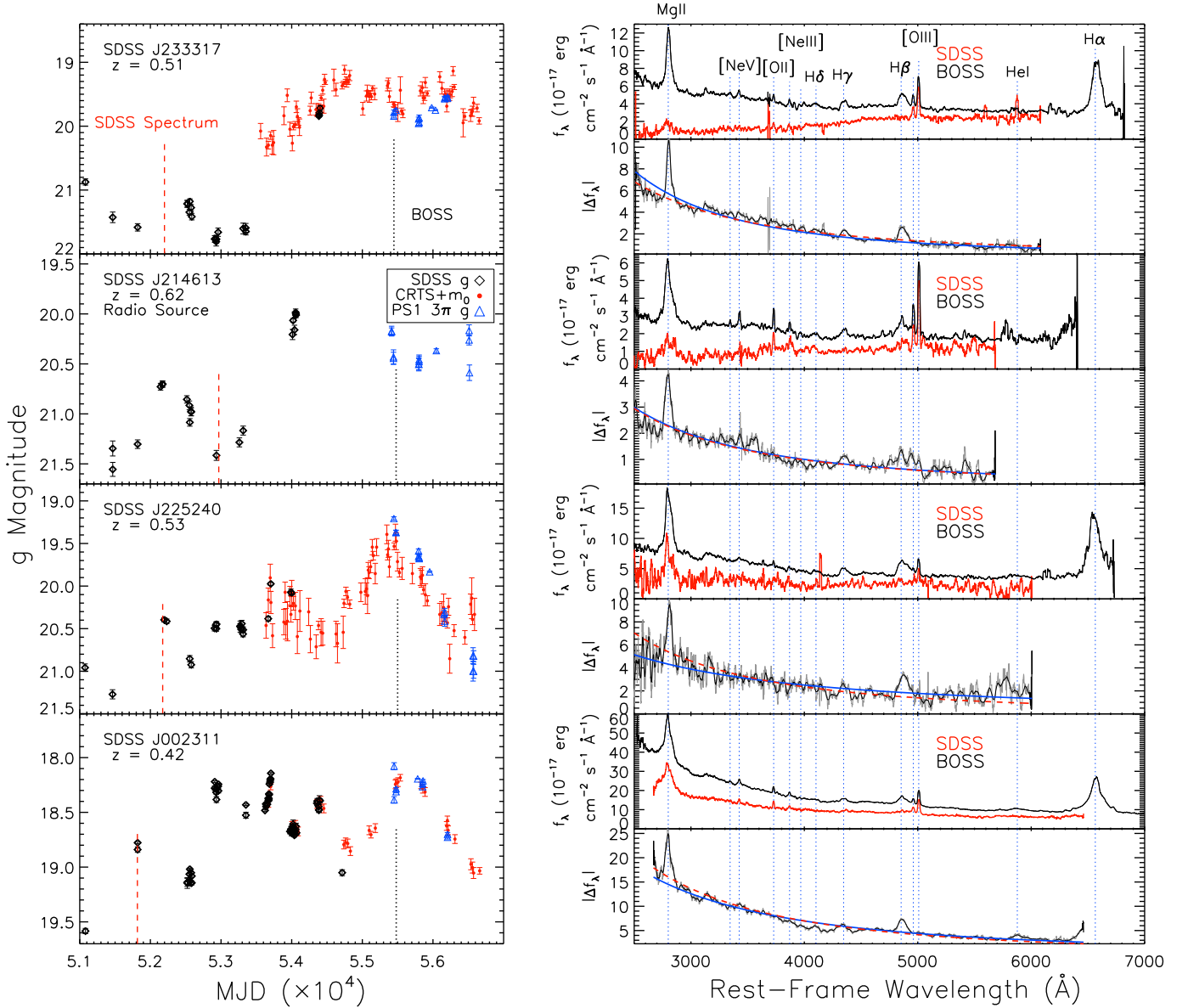


Figure 4. Quasars that show evidence for emerging BELs. The light curves in the left panel show the SDSS g -band (black diamonds), PS1 g -band (blue triangles), and CRTS photometry (red dots). The right panels show the SDSS and BOSS spectra in red and black, respectively, with epochs indicated by the (color-coded) vertical dotted lines in the light curve. The flux difference $|\Delta f_\lambda|$ between the BOSS and SDSS spectra is shown in the right lower subpanels, where the blue curve is the best-fit power-law $f_\nu \propto \nu^\beta$, and the red-dashed curve is a power-law with $\beta = 1/3$ which is expected for a standard thin disk.

uary 2015 (MJD = 57036) by Ruan et al. (2015) using the 3.5m telescope at the Apache Point Observatory (APO), and it is presented in the Appendix of that paper. The $H\beta$ BEL is present in the APO spectrum but diminished with respect to the SDSS spectrum. However, assuming that the measured BOSS flux is accurate, the APO spectrum was obtained when the object had rebrightened.

4.3 Both Appearing and Disappearing BELs

One object, SDSS J022556.07+003026.7 (hereafter J0225+0030), shows a significant evolution of the BELs as the source dims and rebrightens (see Fig. 6). The multiple

BOSS spectra⁸ reveal a complete disappearance and re-emergence of $H\beta$, although this is at low significance due to low signal-to-noise. $MgII$ shows a similar behavior, but it retains a broad component throughout. While outside the range of the SDSS spectrum, in the BOSS spectra the broad $H\alpha$ component shows a clear increase over the course of just one year, going from MJD=55445 (in black) to 55827 (in cyan). Similar rapid BEL changes have also been observed in

⁸ J0225+0030 was observed multiple times due to it being on the extra deep BOSS plates 3615 and 3647, see http://www.sdss.org/dr12/spectro/special_plates/. There were 12 additional epochs of spectroscopy which are not shown in Fig. 6.

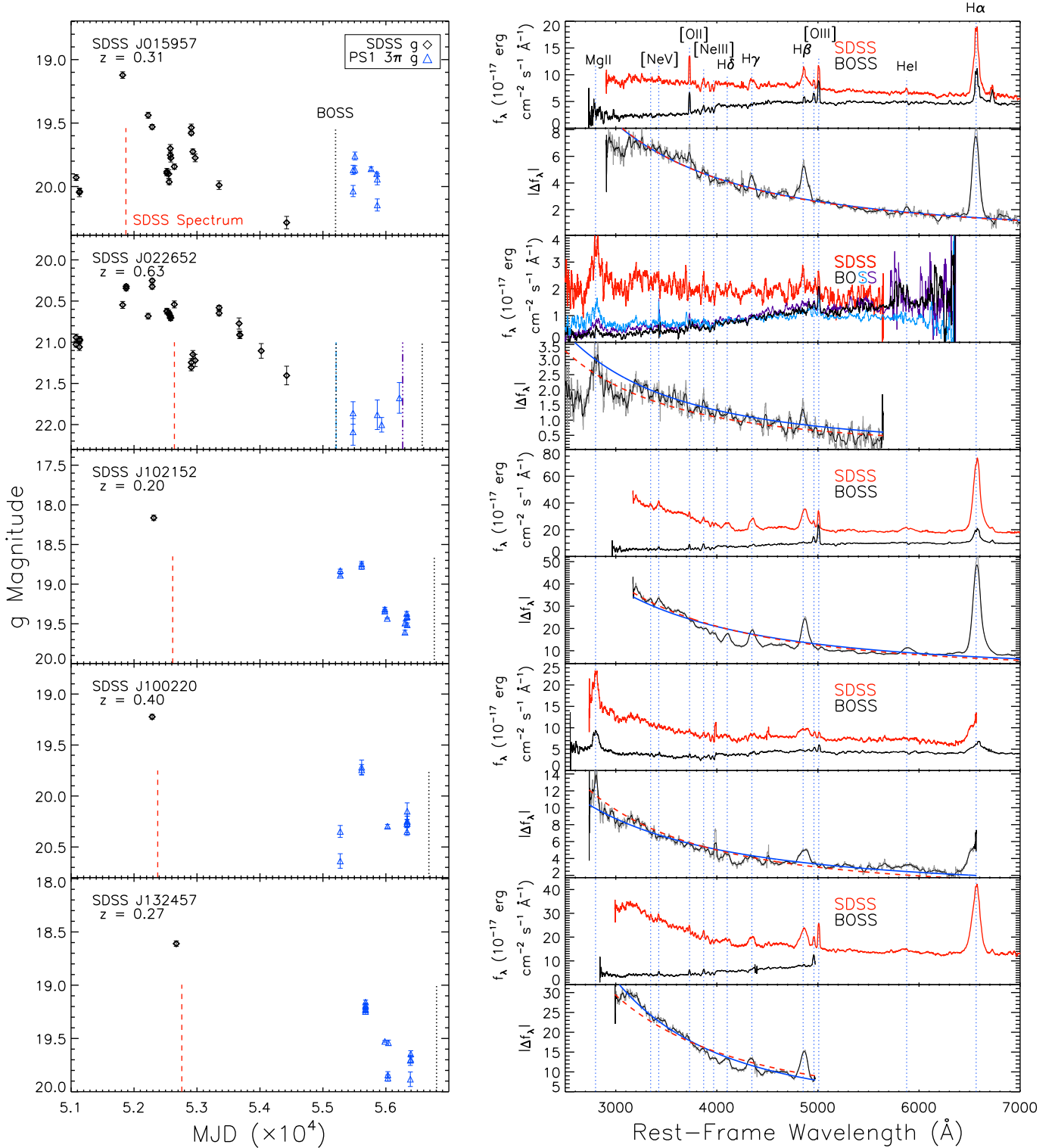


Figure 5. Quasars with disappearing BELs. The top panels show J0159+0033, which was discovered in [LaMassa et al. \(2015\)](#). The cyan and purple spectra in the second (right) panel show additional BOSS epochs at MJD= 55209 and 56267, respectively.

Seyfert galaxies such as NGC 7603 ([Tohline & Osterbrock 1976](#)) and Mkn 110 ([Bischoff & Kollatschny 1999](#)). In the MgII BEL profile shown in the lower left panel, the red wing diminishes faster than the blue wing which is broadly consistent with infalling gas. Such profile changes may

provide a tool to study the structure of the BLR and warrants a future detailed study.

Here, we are interested in the response of the Mg II line to the underlying NUV continuum in comparison to what is typically observed, since atypical behavior may indicate a

rare, more extreme event. We measure the EW of Mg II and find it to be constant ($\approx 100\text{\AA}$) over the large drop in local continuum flux going from $5.2 \times 10^{-17} \text{ erg cm}^{-2} \text{ s}^{-1} \text{ \AA}^{-1}$ in MJD=52944 to $0.9 \times 10^{-17} \text{ erg cm}^{-2} \text{ s}^{-1} \text{ \AA}^{-1}$ in 55445. For the few reverberation mapped sources with Mg II coverage, the Mg II line is typically unresponsive (e.g., Clavel et al. 1991; Krolik et al. 1991; Goad et al. 1993; Cackett et al. 2015), meaning that the line flux is constant as the continuum level varies. The result is an intrinsic Baldwin effect where the EW decreases with increasing continuum flux in a given AGN. Since the Mg II EW remains constant (leading to a negligible Baldwin effect, as seen for an ensemble of objects in Dietrich et al. 2002), it seems that the Mg II BEL response in J0225+0030 is more pronounced than in typical AGN.

We elaborate on J0225+0030 in Section A3.

4.4 Continuum Changes

While the majority of highly-variable quasars in our search did not exhibit emerging or disappearing BELs, they often showed clear changes in the continuum slope in a bluer-when-brighter fashion, as is expected for quasars⁹ (e.g., Schmidt et al. 2012). In the 10 cases presented here, clear continuum slope changes were observed along with the BEL changes based on the ratio between spectra.

The difference spectra, shown in the lower right subpanels of Figs 4–6, eliminate any underlying host galaxy light which is present in both spectra and reveal the SED of the variable component. Aside from the features resulting from the BEL change, the $|\Delta f_\lambda|$ curves are well-described by a power-law of the form $f_\nu \propto \nu^\beta$, and the best-fit power-law is shown as a blue curve. The median best-fit power-law index for the sample is $\beta = 0.2$, with an root-mean-square value 0.4. The red dashed curves show a $f_\nu \propto \nu^{1/3}$ power law expected for a standard thin disk, and the difference spectra for all 10 objects appear qualitatively consistent with this form. Note that in some cases, $|\Delta f_\lambda|$ deviates from the power-law at the shortest wavelengths (e.g., top two panels of Fig. 5), but this is likely due to a relatively increased noise level in the SDSS spectrum.

It is well-known that AGN spectra do not typically follow the $f_\nu \propto \nu^{1/3}$ form expected for a standard thin disk in the optical; only the NIR polarized continuum has been shown to agree with this prediction (Kishimoto et al. 2003). This is true for our final sample as well (the median $\beta \approx -1$ in the high-luminosity state). However, $|\Delta f_\lambda|$ for all 10 objects follows a power-law that is much more consistent with $f_\nu \propto \nu^{1/3}$ than the individual spectra. This implies that the variable component is related to the thermal accretion disk, which might be expected if there was a change in the temperature structure of the accretion disk due to a change in viscous heating or irradiating flux.

⁹ We do not quantify the color changes for the overall sample of 1011 objects, as this is outside the scope of the present work. For such a study, we refer readers to Ruan et al. (2014).

Name (SDSS J)	z	Max($ \Delta g $) (mag)	DR7 QSO?	Found here?
012648.08–083948.0 ^a	0.198	0.78 ± 0.03	×	×
015957.64+003310.4 ^b	0.312	1.16 ± 0.06	✓	✓
101152.98+544206.4 ^c	0.246	1.51 ± 0.02	✓	×
233602.98+001728.7 ^a	0.243	1.59 ± 0.13	×	×

Table 3. Previously reported changing-look quasars ($z > 0.1$).
^aFound by Ruan et al. (2015). ^bFound by LaMassa et al. (2015).
^cFound by Runnoe et al. (2015).

4.5 Comparison to Previously Reported Changing-Look Quasars

In Table 3, we list four previously reported changing-look quasars (at $z > 0.1$), including J0159+0033. J012648.08–083948.0 and J233602.98+001728.7 are not in DR7Q and therefore are not in our parent sample. These two objects were found by Ruan et al. (2015) in an archival search for objects whose pipeline spectroscopic classifications changed between epochs of spectroscopy. Therefore, their search was sensitive to only the most dramatic changes in spectral state, whereas our variability-based selection is sensitive to dramatic transitions as well as more subtle changes in AGN type. However, while J233602.98+001728.7 shows enough variability to be included in our sample, J012648.08–083948.0 only shows a 0.78 mag dimming going from SDSS to PS1. This suggests that our variability criterion of $|\Delta g| > 1.0$ mag is too restrictive.

The Ruan et al. (2015) sample selects objects that change their "CLASS" classification, where the CLASS parameter is from the 1-D SDSS pipeline (see Section 5, Bolton et al. 2012). All the objects in our sample except for two are originally classified as "QSO" and stay classified as CLASS=QSO in their later epoch pipeline classification. The two exceptions are J0159+0033 and J132457.29+480241.2. However, the latter source was not considered in the end to be a changing-look quasar by Ruan et al. due to reasons described in the Appendix of that paper.

The Time Domain Spectroscopic Survey of SDSS-IV (TDSS; Morganson et al. 2015) is obtaining repeat spectra for quasars showing $|\Delta g| > 0.7$ mag variability, and is likely to find a more complete sample of changing-look quasars. J101152.98+544206.4, discovered by TDSS (Runnoe et al. 2015), is in DR7Q but does not have a spectrum in DR12. Had it been observed in SDSS-III, we would have recovered this object since it is 1.5 mag dimmer in PS1 ($g = 19.879 \pm 0.014$ at MJD = 55838.170) with respect to SDSS.

5 DISCUSSION

AGN are known to be variable phenomena. However, it is only relatively recently that multiple spectra of the same AGN at high- z have become available, mainly due to large spectroscopic surveys such as the SDSS. Moreover, noting changes in these spectra of AGN gives direct observational evidence and insight to the physical processes that are happening in the AGN.

One key result from our systematic search is that us-

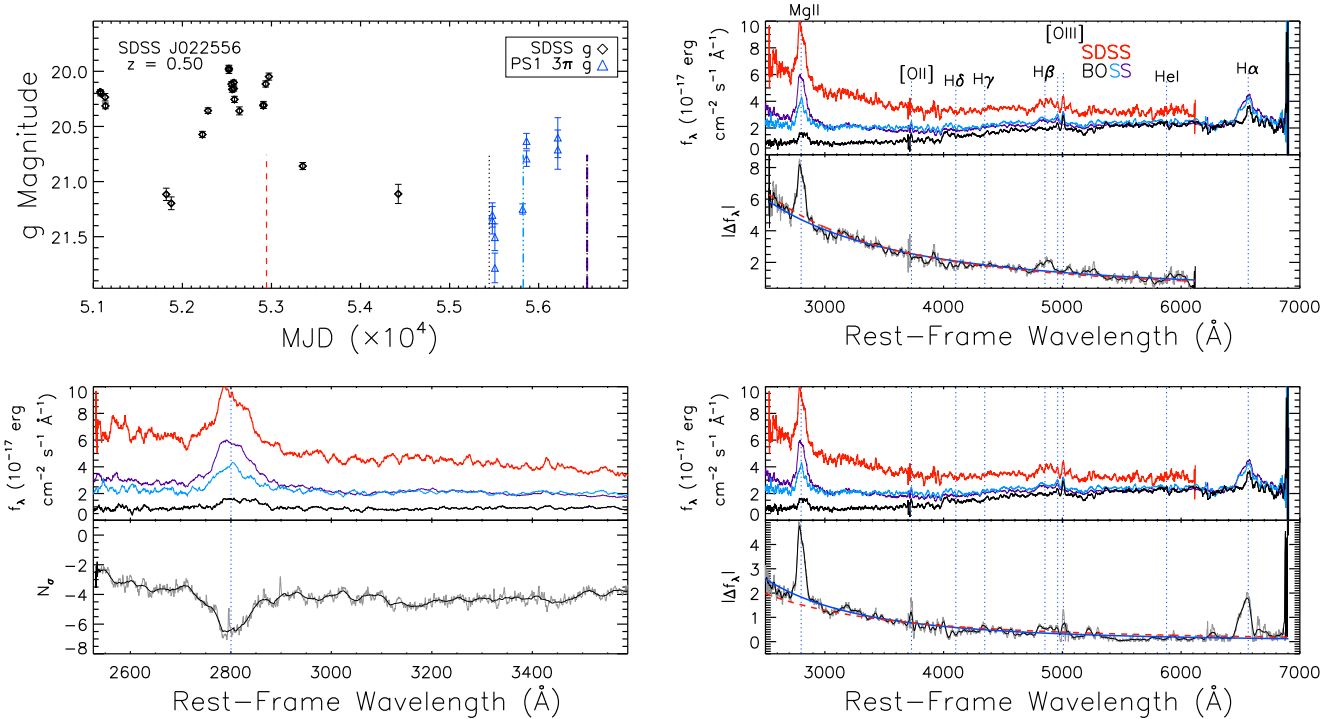


Figure 6. A quasar exhibiting disappearing and reappearing BELs. In the lower left panel, a zoom-in on the Mg II line shows profile changes, and the flux deviation $N_\sigma = (f_2 - f_1)/\sqrt{\sigma_2^2 + \sigma_1^2}$ between the early BOSS (black, f_2) and SDSS (red, f_1) spectra is shown in the bottom panel. The lower right panel is identical to the upper right panel except that the flux difference $f_3 - f_2$ between the latest BOSS (purple, f_3) and earlier BOSS (black, f_2) spectra is shown. The epochs for the red, black, cyan, and purple spectra are MJD = 52944, 55445, 55827, and 56544, respectively.

ing a variability cut seems to be one effective way of finding changing-look quasars. Our base sample is DR7Q, of which 6348 (6%) satisfy the photometric selection described in Section 3. Of these, 1011 objects are reobserved with BOSS, and 10 (1%) show BEL (dis)appearances and reside in the redshift range $0.20 < z < 0.63$. We may be biased toward finding changing-look behavior at $z < 0.8$ since beyond this the H β line is no longer in the SDSS spectrum, and significant changes were most commonly seen in this line. The lack of significant changes in the C IV and Mg II lines may be due to the fact that C IV is affected by winds (Richards et al. 2011) and that Mg II has a relatively weak responsivity (Goad et al. 1993; Cackett et al. 2015).

A second key result from our study is that the difference spectra for our final sample of 10 changing-look quasars are more consistent with the naively expected $f_\nu \propto \nu^{1/3}$ power-law for a thin disk (Shakura & Sunyaev 1973) than the individual spectra. This suggests that the variable component has an SED similar to an accretion disk, and that the reddening in the quasar host galaxy must be small. Furthermore, whatever is causing a BEL (dis)appearance must be linked to an emerging (diminishing) continuum. Indeed, the BELs track the blue continuum change on rest-frame timescales as short as 255 days in J0225+0030 (Section 4.3).

“Outbursts” associated with BEL appearance could be due to changing obscuration, changing accretion rate, or transient behavior such as a tidal disruption event (TDE) or microlensing. Presumably because of the relatively low redshifts, these are not microlensing events (see

Lawrence et al. 2012, for larger amplitude and typically more distant AGN flares). While a TDE could explain J0159+0033 (Merloni et al. 2015), such a flaring episode is ruled out for at least some other objects presented here. For example, the light curve in the top panel of Fig. 4 shows that the luminosity has remained in the high state for the last 2000 days (observed frame) instead of decaying with a $t^{-5/3}$ form expected for a TDE (e.g., Evans & Kochanek 1989; Gezari et al. 2012; Guillochon et al. 2014). Furthermore, TDEs should only remain in the high state for a few months (e.g., Gezari et al. 2012), unlike what is observed here. In addition, the narrow emission lines are present in the early states for each source, which would be too fast of a large-scale response for a TDE (as pointed out by Runnoe et al. 2015; Ruan et al. 2015). Therefore, we limit the following discussion to the first two possible scenarios.

5.1 Observed Timescales for BEL (Dis)appearance

One feature which may help guide physical interpretations is the timescale associated with a spectral state change. As such, we would like to place an upper limit on the *fastest* timescales associated with BEL (dis)appearance. Due to the nature of the SDSS and PS1, we lack a complete sampling of timescales and are prone to selection effects imposed by the timing of both the photometric and (especially the) spectroscopic observations. In Fig. 7, we show the probability p which is simply the ratio of changing-look quasars to the

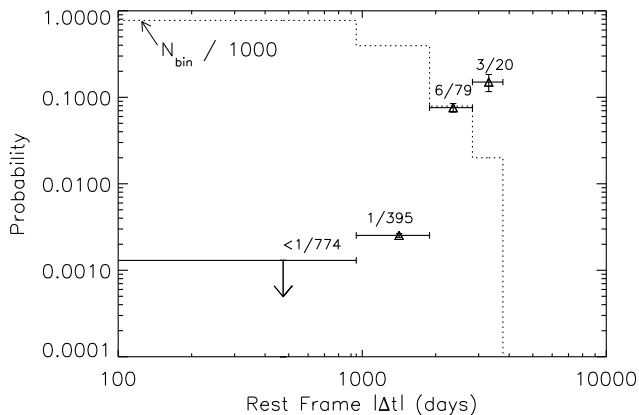


Figure 7. Probability, p , of BEL (dis)appearance as a function of rest-frame time lag, based on our sample (see text). The errors in p are computed as $p/\sqrt{N_{\text{bin}}}$, where N_{bin} (shown as the normalized, dotted histogram) is the number of highly variable quasars with repeat spectra (red open data points in Fig. 1) which fall in each time bin. None of our 10 objects have $|\Delta t| < 1000$ days, so for this bin we only show an upper limit corresponding to < 1 object. The ratio of changing-look objects to N_{bin} is listed in each bin.

highly variable sample with repeat spectra, i.e., the ratio of blue crosses to red open circles in each of the four time bins shown in the bottom panel of Fig. 1. Out of the highly variable objects with repeat spectra, we find the highest probability for changing-look behavior on rest-frame timescales of 2000–3000 days and 3000–4000 days ($p = 0.076 \pm 0.009$ and $p = 0.15 \pm 0.03$, respectively). When restricted to the redshift range $0.2 < z < 0.63$, p increases to $p = 0.113 \pm 0.016$ and $p = 0.18 \pm 0.04$, respectively. Note that p will be higher for the subsample with *spectroscopic* epochs spanning a > 1 mag change (i.e., those showing a > 1 mag change from one spectral epoch to the next, shown by the red open circles above the dashed line in Fig. 1) – this subsample is more representative of the objects in which we could have observed changing-look behavior. However, the size of this subsample is too small to make any statistical conclusions. Along with being biased by the sparse sampling of spectroscopic epochs, we are also likely biased toward long rest-frame timescales given that $H\beta$ is only visible at $z < 0.8$. Fig. 7 suggests that the fraction of changing-look quasars rises to 0.2 at $\Delta t \sim 10$ yr; therefore, future surveys are needed to determine if the fraction of changing-look quasars continues to rise on even longer timescales.

While the timescales for BEL changes explored in Fig. 7 are limited to the timing of spectroscopic observations, seven of our objects have S82 light curves, which provide more information on the timescales over which the transitions may have occurred. In general, the light curves show strong increases in flux over 1000 days in the observed frame (or roughly two years in the quasar rest frame; Fig. 4), but strong decreases in flux over considerably longer timescales (several years in the observed frame; top two panels of Fig. 5). The light curve for J0225+0030 (Fig. 6) shows a rise over less than a year in the quasar rest frame following a slow decline over 5 years in the rest frame.

5.2 A Change in the Central Engine?

To explore a physical scenario where the amount of available ionizing flux from the central engine has changed, we must consider both the timescale for BEL response as well as the timescale for the continuum variability. In the first case, since BELs result from photoionization (e.g., Peterson 1993), they should respond on the light crossing timescale $t_{\text{lt}} = R_{\text{BLR}}/c$ days, where R_{BLR} is the radius of the BLR. Using the $R - L$ relation calibrated by Bentz et al. (2013), the BLR size is estimated to be $R_{\text{BLR}} = 2954 R_S M_8^{-1} L_{44}^{0.533}$, where $M_8 = M_{\text{BH}}/(10^8 M_\odot)$ is the mass of the central super-massive black hole in units of $10^8 M_\odot$, $L_{44} = \lambda L_\lambda(5100)/(10^{44} \text{ erg s}^{-1})$, and R_S is the Schwarzschild radius $R_S = 2GM_{\text{BH}}/c^2$. This gives $t_{\text{lt}} = 34 L_{44}^{0.533}$ days, similar to the observed BEL lags in reverberation mapping (RM), although the lags are typically shorter since the majority of the ~ 50 AGN studied through RM have lower luminosities.

One assumption in RM studies is that the structure of the BLR remains stable over the duration of the experiment. For Seyferts, the optical continuum variations are typically a factor 1.3 over rest-frame timescales of \sim months (e.g., Edelson et al. 2015). The photometric variability presented here is more dramatic in comparison: on average by a factor 4 in g -band flux over seven years in the rest frame. Furthermore, we observe a stronger Mg II response in J0225+0030 over 4.5 years in the rest frame (Section 4.3) than typical in RM studies (e.g., Cackett et al. 2015), which might be expected if the source of ionizing photons has significantly diminished. In this case, the BLR may have time to adjust its overall structure in response to such large changes in ionizing flux, and BEL changes might be expected on the dynamical timescale of the BLR. For typical Seyfert galaxies, $t_{\text{dyn}} \approx R_{\text{BLR}}/\Delta V \approx 3$ to 5 years (Peterson 2006), where ΔV is a typical cloud velocity. This timescale will be slightly longer for higher-luminosity quasars, since $t_{\text{dyn}} \propto L^{3/4} M_{\text{BH}}^{-1/2}$, assuming Keplerian rotation and that $R_{\text{BLR}} \propto L^{1/2}$ for photoionized lines. The time between SDSS and BOSS spectra is long enough so that a dynamical response of the BLR cannot generally be ruled out for our sample.

Regardless of what is happening in the broad line region, it is clear that the BELs track a large change in continuum level flux. The timescale that might be associated with an accretion rate change is the viscous, or “radial inflow” timescale (see e.g., Krolik 1999). Indeed, Elitzur et al. (2014) provide a scenario where AGN evolve naturally from Type 1 to 1.2/1.5 to 1.8/1.9 as the accretion rate diminishes. Using Equation 5 in LaMassa et al. (2015) and scaling the Eddington parameter λ_{Edd} and M_{BH} to the measured values for J1021+4645 from Shen et al. (2011), we obtain:

$$t_{\text{inff}} = 5 \times 10^4 \left[\frac{\alpha}{0.1} \right]^{-1} \left[\frac{\lambda_{\text{Edd}}}{0.05} \right]^{-2} \left[\frac{\eta}{0.1} \right]^2 \left[\frac{r}{50 R_S} \right]^{7/2} \left[\frac{M_8}{2.1} \right] \text{yr}. \quad (1)$$

Here, α is the disk viscosity parameter, η is the accretion efficiency, and r is the accretion disk radius (assumed to be $50 R_S$ for optical disk emission). The value of t_{inff} may be a several times shorter based on magneto-hydrodynamical simulations (e.g., Krolik et al. 2005), but this is still too long to explain the continuum variability of all sources presented

here (see the Appendix for the individual physical parameters and t_{inff} estimates). The source J022652.24–003916.5 has a relatively low mass and therefore is expected to have a relatively short t_{inff} of ~ 56 yr, still an order of magnitude too long to explain the observed optical variability. Furthermore, [LaMassa et al. \(2015\)](#) point out that t_{inff} should be considerably longer in the dim state since $t_{\text{inff}} \propto \lambda_{\text{Edd}}^{-2}$, and thus the dimming timescale should be shorter than the recovery timescale. However, the S82 light curves suggest the opposite behavior: the objects with appearing BELs show brightening on much shorter timescales than is plausible for the optical viscous timescale in the dim states of these AGN.

Nevertheless, t_{inff} might still be an appropriate timescale if the optical flux contains reprocessed emission from the EUV, where t_{inff} may be orders of magnitude shorter. In the disk reprocessing scenario, the disk surface is irradiated by EUV/X-ray photons coming from a central source on the light travel timescale, and the re-emitted UV/optical flux can vary on the shorter timescales associated with the central region. This “lamp post” model (e.g., [Berkley et al. 2000](#); [Martocchia et al. 2002](#)) is supported by observations of quasar microlensing (e.g., [Morgan et al. 2008](#); [Mosquera et al. 2013](#); [MacLeod et al. 2015](#)), which show that the X-rays originate from projected radii near the inner edge of the accretion disk. Indeed, multi-wavelength observations of NGC 4051 indicate that $\sim 25\%$ of the UV variance is caused by thermal reprocessing ([Alston et al. 2013](#)). In the disk reprocessing model of [Cackett et al. \(2007\)](#), the disk temperature T_0 at a fiducial radius R_0 is regulated by both local viscous heating and irradiation:

$$T_0^4 = T_{\text{inff}}^4 + T_{\text{irr}}^4 = \frac{3GM_{\text{BH}}\dot{M}}{8\pi\sigma R_0^3} + \frac{L_X(1-A)h}{4\pi\sigma R_0^3}, \quad (2)$$

where L_X is the lamp post luminosity at a height h above the black hole, and A is the disk albedo. In this case, the temperature-radius profile of the disk would rise and fall with changes in either local accretion rate or irradiation, and this would produce a difference spectrum that remains an $f_\nu \propto \nu^{1/3}$ power-law ([Cackett et al. 2007](#)), similar to what we observe in the objects presented here. Note that the fraction of reprocessed flux that is re-emitted toward the interior of the disk can modify its internal structure, but this effect is negligible unless L_X is similar to the bolometric luminosity of the quasar ([Collin 2001](#)).

5.3 Variable Obscuration?

In the case of variable extinction, a passing cloud may obscure the BLR on a characteristic crossing timescale t_{cross} . In the simplest scenario, such an event must account for the disappearing BELs and thermal continuum. One possibility is a passing isolated BLR cloud obscuring the continuum emitting region as seen by us and by the (remainder of the) BLR. While this scenario is viable in the X-rays where the continuum emitting source is relatively compact (e.g., [Risaliti et al. 2009](#)), the UV/optical continuum emitting region being significantly larger makes this scenario less likely. But the timescale for such a crossing event is reasonable: $t_{\text{cross, BLR cloud}} = 84M_8^{-1/2}L_{44}^{3/4}$ days assuming a Keplerian orbit for a BLR cloud passing at $r_{\text{orb}} = R_{\text{BLR}} = 2954R_S M_8^{-1}L_{44}^{1/2}$ in front of the continuum source, where

the latter has a radius $r_{\text{src}} = R_{\text{BLR}}/60$ (see Equation 4 in [LaMassa et al. 2015](#)).

Another possibility is that the entire UV/continuum emitting region and BLR is obscured; this might be expected if the distribution of dust lying at the outskirts of the BLR is patchy (e.g., [Nenkova et al. 2008a,b](#); [Elitzur 2012](#)). In this case, reasonable values would be $r_{\text{src}} = R_{\text{BLR}} = 2954R_S M_8^{-1}L_{44}^{1/2}$ and $r_{\text{orb}} = 3R_{\text{BLR}}$ for dust at r_{orb} to obscure a significant portion of the BLR ([LaMassa et al. 2015](#)). This gives $t_{\text{cross, dust}} = 24M_8^{-1/2}L_{44}^{3/4}$ yr.

The t_{cross} estimates are listed in Table A1 for each source. The $t_{\text{cross, BLR cloud}}$ estimates are shorter than the observed brightening and dimming timescales for all sources, but since the size and structure of BLR clouds is uncertain, these timescales may be longer than predicted. The $t_{\text{cross, dust}}$ values are too long to explain the light curve behavior of these sources but are in many cases of the same order as the observed timescales. For example, the source SDSS J233317.38-002303.4 has the shortest $t_{\text{cross, dust}}$ estimate of 4.5 yrs (based on the luminosity in the bright state), but the observed brightening happens over 2.7 yr in the rest frame (top panel of Fig. 4). For the densely monitored object J0225+0030, the predicted dust crossing timescale is an order of magnitude too long to explain the rebrightening around MJD= 55500 (Fig. 6). Nevertheless, we further investigate the plausibility of variable obscuration by considering simple dust reddening models.

5.3.1 Dust Reddening Test

We consider whether an obscuration event can account for the spectral changes by applying dust reddening to the observed spectra. In particular, we simply apply Milky Way (MW) and Small Magellanic Cloud (SMC) dust reddening curves to the bright-state spectra and see whether we can reproduce the BEL disappearance in the faint-state spectra. This test is demonstrated here for SDSS J1021+4645, which has high quality spectra that show the most dramatic transition from a Type 1.0 AGN in SDSS to a Type 1.9 AGN in BOSS among our objects.

Assuming the SDSS spectrum for SDSS J1021+4645 is the intrinsic, unabsorbed flux, we estimate $A_V = 0.95$ by taking the magnitude difference between the SDSS and BOSS spectra at the effective wavelength of the Johnson V band. The SDSS spectrum is then multiplied by a factor $10^{-A_\lambda/2.5}$, where $A_\lambda = E(\lambda - V) + A_V$, $E(\lambda - V) = k(\lambda)E(B - V)$, and $k(\lambda)$ is an extinction curve. For SMC-like extinction, we tried the four different models in Table 5 of [Gordon & Clayton \(1998\)](#), which use the parametrization in Equation 2 of [Fitzpatrick & Massa \(1990\)](#). We find that the AzV 214 model ($R_V = 2.75$) produces an absorbed spectrum most similar to the observed BOSS spectrum among the four fits, and the result is shown in Fig. 8. We also try a MW-like extinction curve ($R_V = 3.1$; [Seaton 1979](#)), and assume $A_V = 0.95$ as before. Note that the SDSS spectrum will contain a host galaxy component that is not modeled here. However, we are not interested in reproducing the detailed continuum shape of the BOSS spectrum but rather the BEL change, so we leave a detailed spectral modeling for a future study as it should not affect our final conclusions.

There are two points to note from the simple extinction

tests in Fig. 8. First, the SMC-like extinction curve does a better job than the MW-like extinction curve at removing the blue part of the continuum in the SDSS spectrum. Second, while the SMC-like extinction model can qualitatively explain the continuum change going from SDSS to BOSS, neither dust model can explain the disappearance of the BELs. In particular, the $H\beta$ BEL remains prominent in the absorbed versions of the SDSS spectrum. This latter point is similar to what LaMassa et al. (2015) find for J0159+0033, where the observed $H\alpha$ BEL is much stronger than it should be if reddening alone is responsible for the spectral change. LaMassa et al. (2015) also find that archival X-ray spectra in the bright and faint states of J0159+0033 both appear unabsorbed.

We reach the same conclusion when repeating the above exercise for the other nine sources, using each pair of spectra listed in Table 2: if reddening alone could account for the observed spectral changes, then the broad component of $H\beta$ should be present in the faint-state spectrum on top of the host galaxy flux. However, the broad line flux is instead negligible in each case. Therefore, simple dust reddening models fail to simultaneously account for the diminished continuum and broad Balmer line components in all ten sources. In principle, one could employ a different A_V for the BELs than for the continuum to explain the optical spectral change, but this leads to a more complicated physical scenario than we explore here.

6 CONCLUSIONS

We have presented the first systematic search for changing-look quasars using data from the SDSS and PS1 3π . Out of 6348 quasars from DR7Q that exhibit $|\Delta g| > 1$ mag variability over the SDSS and PS1 photometric epochs, 1011 have been reobserved with BOSS. Of these, we visually identify 10 changing-look quasars, extending the known population of changing-look AGN to $z = 0.63$.

Our search has yielded the following:

- four objects with appearing BELs corresponding to > 1 mag increases in flux in the g -band;
- five objects with disappearing BELs and declining light curves, which includes the changing-look quasar discovered in LaMassa et al. (2015), and an even more dramatic transition from a Type 1.0 to 1.9 AGN in the object J1021+4645 (with a flux deviation per spectral pixel of 8σ for $H\beta$);
- one object showing evidence of both disappearing and appearing BELs on timescales less than a year in the quasar frame;
- an SED of the variable component resembling thermal emission from an accretion disk;
- that $\sim 15\%$ of quasars that have varied by $|\Delta g| > 1$ mag at some point in their light curve display changing-look behavior on rest-frame timescales of 3000–4000 days;
- that a change in ionizing flux from the central engine coupled with disk reprocessing is a more likely explanation than variable obscuration in all cases, based on timescale arguments and simple dust reddening models.

While the detailed physical mechanisms behind BEL changes may be complicated to understand and model, changing-look AGN can provide a laboratory to study the

relationship between emission at different wavelengths, as the entire system may respond to a strong increase or decline in available ionizing flux. As a prime example, following an outburst in the X-ray emission in the local Seyfert NGC 2617, Shappee et al. (2014) were able to use the variability across several wavebands (spanning X-rays–NIR) to map out the structure of the accretion disk and argue for illumination of the disk by the X-ray source. The observations presented here support this scenario, although we cannot rule out a change in obscuration without more complex models for the structure and size of the intervening material.

Our results indicate that photometric variability might be one of the best ways to efficiently find changing-look quasars in current datasets. Furthermore, with well-sampled light curves provided by the S82 survey, extreme behavior can be more readily identified, as demonstrated by the higher yield of changing-look objects from S82 presented here. Therefore, future time domain surveys such as the Large Synoptic Survey Telescope (Ivezic et al. 2008; LSST Science Collaboration et al. 2009), PS1 and PS2 (Chambers 2014), as well as the ongoing All-Sky Automated Survey for SuperNovae (Shappee et al. 2014), should provide excellent datasets in which to search for interesting targets for spectroscopic follow-up. Based on the observations in Shappee et al. (2014) and LaMassa et al. (2015), extreme X-ray variability may also help identify changing-look AGN candidates among samples of extremely optically-variable quasars. Furthermore, a multi-wavelength monitoring campaign of these objects would be useful for interpreting the nature of such transitions. However, since it is unclear how rare these transitions are at any given timescale, further work is necessary for determining the best strategy for follow-up monitoring. The TDSS project of SDSS-IV (Morganson et al. 2015) has already initiated a similar search to the one presented here, extending the search criteria down to $\Delta g > 0.7$ mag, and should place more stringent limits on the frequency of such events. On the longer term, the Dark Energy Spectroscopic Instrument (DESI) will survey $\sim 2.4 \times 10^6$ quasars (Levi et al. 2013), providing ample opportunity for obtaining additional spectroscopic epochs for highly-variable AGN.

ACKNOWLEDGEMENTS

We acknowledge Marco Lam and Nigel Hambly for assistance with and maintaining the local PS1 DVO database. We also acknowledge Isabelle Pâris for help with checking which of our objects were in the SDSS-III BOSS Quasar catalog. We thank the reviewer for valuable suggestions that improved the paper. CLM acknowledges support from the STFC Consolidated Grant (Ref. St/M001229/1). NPR acknowledges support from the STFC and the Ernest Rutherford Fellowship scheme. KH acknowledges support from STFC grant ST/M001296/1.

Funding for the SDSS and SDSS-II has been provided by the Alfred P. Sloan Foundation, the Participating Institutions, the National Science Foundation, the U.S. Department of Energy, the National Aeronautics and Space Administration, the Japanese Monbukagakusho, the Max Planck Society, and the Higher Education Funding Council for England. The SDSS Web Site is <http://www.sdss.org/>.

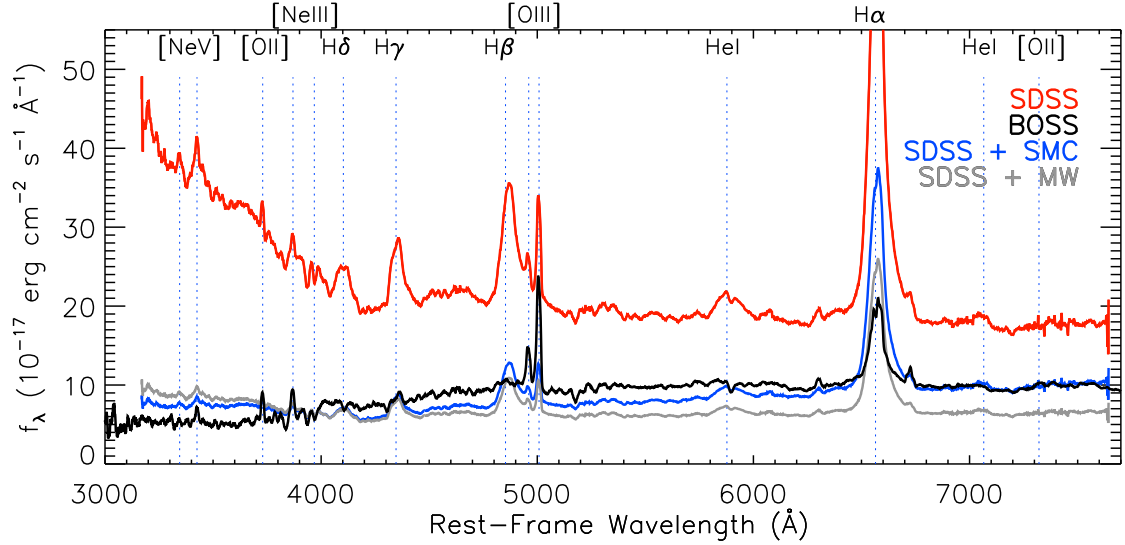


Figure 8. SDSS J1021+4645, showing a dramatic transition from a Type 1.0 AGN in SDSS (shown in red) to a Type 1.9 AGN in BOSS (shown in thick black). The red spectrum shows the observed SDSS flux; the grey and blue spectra show extinguished versions of the SDSS spectrum using a MW and an SMC extinction curve, respectively (see text for details). Applying reddening to the SDSS spectrum is inadequate for reproducing the BOSS spectrum, such that a simple extinction scenario can be ruled out as an explanation for the transition.

The SDSS is managed by the Astrophysical Research Consortium for the Participating Institutions. The Participating Institutions are the American Museum of Natural History, Astrophysical Institute Potsdam, University of Basel, University of Cambridge, Case Western Reserve University, University of Chicago, Drexel University, Fermilab, the Institute for Advanced Study, the Japan Participation Group, Johns Hopkins University, the Joint Institute for Nuclear Astrophysics, the Kavli Institute for Particle Astrophysics and Cosmology, the Korean Scientist Group, the Chinese Academy of Sciences (LAMOST), Los Alamos National Laboratory, the Max-Planck-Institute for Astronomy (MPIA), the Max-Planck-Institute for Astrophysics (MPA), New Mexico State University, Ohio State University, University of Pittsburgh, University of Portsmouth, Princeton University, the United States Naval Observatory, and the University of Washington.

Funding for SDSS-III has been provided by the Alfred P. Sloan Foundation, the Participating Institutions, the National Science Foundation, and the U.S. Department of Energy Office of Science. The SDSS-III web site is <http://www.sdss3.org/>.

SDSS-III is managed by the Astrophysical Research Consortium for the Participating Institutions of the SDSS-III Collaboration including the University of Arizona, the Brazilian Participation Group, Brookhaven National Laboratory, Carnegie Mellon University, University of Florida, the French Participation Group, the German Participation Group, Harvard University, the Instituto de Astrofísica de Canarias, the Michigan State/Notre Dame/JINA Participation Group, Johns Hopkins University, Lawrence Berkeley National Laboratory, Max Planck Institute for Astrophysics, Max Planck Institute for Extraterrestrial Physics, New Mexico State University, New York University, Ohio State University, Pennsylvania State University, University

of Portsmouth, Princeton University, the Spanish Participation Group, University of Tokyo, University of Utah, Vanderbilt University, University of Virginia, University of Washington, and Yale University.

The Pan-STARRS1 Surveys (PS1) have been made possible through contributions of the Institute for Astronomy, the University of Hawaii, the Pan-STARRS Project Office, the Max-Planck Society and its participating institutes, the Max Planck Institute for Astronomy, Heidelberg and the Max Planck Institute for Extraterrestrial Physics, Garching, The Johns Hopkins University, Durham University, the University of Edinburgh, Queen’s University Belfast, the Harvard-Smithsonian Center for Astrophysics, the Las Cumbres Observatory Global Telescope Network Incorporated, the National Central University of Taiwan, the Space Telescope Science Institute, the National Aeronautics and Space Administration under Grant No. NNX08AR22G issued through the Planetary Science Division of the NASA Science Mission Directorate, the National Science Foundation under Grant No. AST-1238877, the University of Maryland, and Eotvos Lorand University (ELTE).

The CSS survey is funded by the National Aeronautics and Space Administration under Grant No. NNG05GF22G issued through the Science Mission Directorate Near-Earth Objects Observations Program. The CRTS survey is supported by the U.S. National Science Foundation under grants AST-0909182 and AST-1313422.

This research has made use of data obtained from the Chandra Source Catalog, provided by the Chandra X-ray Center (CXC) as part of the Chandra Data Archive.

Facilities: SDSS; BOSS; Pan-STARRS1

REFERENCES

- Abazajian K. N., et al., 2009, *ApJS*, **182**, 543
- Ai Y. L., Yuan W., Zhou H. Y., Wang T. G., Dong X.-B., Wang J. G., Lu H. L., 2010, *ApJ*, **716**, L31
- Aihara H., et al., 2011, *The Astrophysical Journal Supplement Series*, **193**, 29
- Alam S., et al., 2015, *ApJS*, **219**, 12
- Alston W. N., Vaughan S., Uttley P., 2013, *MNRAS*, **429**, 75
- Aretxaga I., Joguet B., Kunth D., Melnick J., Terlevich R. J., 1999, *ApJ*, **519**, L123
- Baldwin J. A., Burke W. L., Gaskell C. M., Wampler E. J., 1978, *Nature*, **273**, 431
- Becker R. H., White R. L., Helfand D. J., 1995, *ApJ*, **450**, 559
- Bentz M. C., et al., 2013, *ApJ*, **767**, 149
- Berkley A. J., Kazanas D., Ozik J., 2000, *ApJ*, **535**, 712
- Bischoff K., Kollatschny W., 1999, *A&A*, **345**, 49
- Bolton A. S., et al., 2012, *AJ*, **144**, 144
- Butler N. R., Bloom J. S., 2011, *AJ*, **141**, 93
- Cackett E. M., Horne K., 2006, *MNRAS*, **365**, 1180
- Cackett E. M., Horne K., Winkler H., 2007, *MNRAS*, **380**, 669
- Cackett E. M., Gültekin K., Bentz M. C., Fausnaugh M. M., Peterson B. M., Troyer J., Vestergaard M., 2015, *ApJ*, **810**, 86
- Chambers K. C., 2014, in *AAS/Division for Planetary Sciences Meeting Abstracts*. p. No. 214.06
- Clavel J., et al., 1991, *ApJ*, **366**, 64
- Cohen R. D., Puetter R. C., Rudy R. J., Ake T. B., Foltz C. B., 1986, *ApJ*, **311**, 135
- Collier S. J., et al., 1998, *ApJ*, **500**, 162
- Collin S., 2001, in Aretxaga I., Kunth D., Mújica R., eds, *Advanced Lectures on the Starburst-AGN*. p. 167 ([arXiv:astro-ph/0101203](https://arxiv.org/abs/astro-ph/0101203))
- Dawson K., et al., 2013, *AJ*, **145**, 10
- Dawson K. S., et al., 2015, preprint, ([arXiv:1508.04473](https://arxiv.org/abs/1508.04473))
- Denney K. D., et al., 2014, *ApJ*, **796**, 134
- Dexter J., Agol E., 2011, *ApJ*, **727**, L24
- Dietrich M., Hamann F., Shields J. C., Constantin A., Vestergaard M., Chaffee F., Foltz C. B., Junkkarinen V. T., 2002, *ApJ*, **581**, 912
- Drake A. J., et al., 2009, *ApJ*, **696**, 870
- Edelson R., et al., 2015, *ApJ*, **806**, 129
- Eisenstein D. J., et al., 2011, *AJ*, **142**, 72
- Elitzur M., 2012, *ApJ*, **747**, L33
- Elitzur M., Ho L. C., Trump J. R., 2014, *MNRAS*, **438**, 3340
- Eracleous M., Halpern J. P., 2001, *ApJ*, **554**, 240
- Evans C. R., Kochanek C. S., 1989, *ApJ*, **346**, L13
- Evans I. N., et al., 2010, *ApJS*, **189**, 37
- Filiz Ak N., et al., 2012, *ApJ*, **757**, 114
- Fitzpatrick E. L., Massa D., 1990, *ApJS*, **72**, 163
- Fukugita M., Ichikawa T., Gunn J. E., Doi M., Shimasaku K., Schneider D. P., 1996, *AJ*, **111**, 1748
- Gaskell C. M., 2007, in Ho L. C., Wang J.-W., eds, *Astronomical Society of the Pacific Conference Series Vol. 373, The Central Engine of Active Galactic Nuclei*. p. 596 ([arXiv:astro-ph/0612474](https://arxiv.org/abs/astro-ph/0612474))
- Gezari S., et al., 2012, *Nature*, **485**, 217
- Gilbert K. M., Peterson B. M., 2003, *ApJ*, **587**, 123
- Goad M. R., O'Brien P. T., Gondhalekar P. M., 1993, *MNRAS*, **263**, 149
- Goad M. R., Korista K. T., Knigge C., 2004, *MNRAS*, **352**, 277
- Goodrich R. W., 1989, *ApJ*, **340**, 190
- Gordon K. D., Clayton G. C., 1998, *ApJ*, **500**, 816
- Grier C. J., et al., 2012, *ApJ*, **755**, 60
- Guillochon J., Manukian H., Ramirez-Ruiz E., 2014, *ApJ*, **783**, 23
- Gunn J. E., et al., 1998, *AJ*, **116**, 3040
- Gunn J. E., et al., 2006, *AJ*, **131**, 2332
- Heckman T. M., Kauffmann G., Brinchmann J., Charlot S., Tremonti C., White S. D. M., 2004, *ApJ*, **613**, 109
- Hogg D. W., Finkbeiner D. P., Schlegel D. J., Gunn J. E., 2001, *AJ*, **122**, 2129
- Inserra C., et al., 2013, *ApJ*, **770**, 128
- Ivezić Ž., et al., 2004a, *Astronomische Nachrichten*, **325**, 583
- Ivezić Ž., et al., 2004b, *Astronomische Nachrichten*, **325**, 583
- Ivezić Z., et al., 2008, preprint, ([arXiv:0805.2366](https://arxiv.org/abs/0805.2366))
- Kaiser N., et al., 2002, in Tyson J. A., Wolff S., eds, *Society of Photo-Optical Instrumentation Engineers (SPIE) Conference Series Vol. 4836, Survey and Other Telescope Technologies and Discoveries*. pp 154–164, [doi:10.1117/12.457365](https://doi.org/10.1117/12.457365)
- Kaiser N., et al., 2010, in *Society of Photo-Optical Instrumentation Engineers (SPIE) Conference Series*. p. 0, [doi:10.1117/12.859188](https://doi.org/10.1117/12.859188)
- Kauffmann G., et al., 2003, *MNRAS*, **346**, 1055
- Kelly B. C., Sobolewska M., Siemiginowska A., 2011, *ApJ*, **730**, 52
- Khachikian E. Y., Weedman D. W., 1971, *ApJ*, **164**, L109
- Kimball A. E., Ivezić Ž., 2014, in Micaeliani A. M., Sanders D. B., eds, *IAU Symposium Vol. 304, IAU Symposium*. pp 238–239, [doi:10.1017/S1743921314003901](https://doi.org/10.1017/S1743921314003901)
- Kinney A. L., Rivolo A. R., Koratkar A. P., 1990, *ApJ*, **357**, 338
- Kishimoto M., Antonucci R., Blaes O., 2003, *MNRAS*, **345**, 253
- Kokubo M., 2015, *MNRAS*, **449**, 94
- Korista K. T., Goad M. R., 2001, *ApJ*, **553**, 695
- Krolik J. H., 1999, *Active galactic nuclei : from the central black hole to the galactic environment*
- Krolik J. H., Horne K., Kallman T. R., Malkan M. A., Edelson R. A., Kriss G. A., 1991, *ApJ*, **371**, 541
- Krolik J. H., Hawley J. F., Hirose S., 2005, *ApJ*, **622**, 1008
- LSST Science Collaboration et al., 2009, preprint, ([arXiv:0912.0201](https://arxiv.org/abs/0912.0201))
- LaMassa S. M., et al., 2015, *ApJ*, **800**, 144
- Lawrence A., 2012, *MNRAS*, **423**, 451
- Lawrence A., Gezari S., Elvis M., Ward M., Smartt S., Smith K., Wright D., 2012, in *European Physical Journal Web of Conferences*. p. 3002, [doi:10.1051/epjconf/20123903002](https://doi.org/10.1051/epjconf/20123903002)
- Levi M., et al., 2013, preprint, ([arXiv:1308.0847](https://arxiv.org/abs/1308.0847))
- Li Y., Yuan W., Zhou H. Y., Komossa S., Ai Y. L., Liu W. J., Boisvert J. H., 2015, *AJ*, **149**, 75
- Luo B., Brandt W. N., Eracleous M., Wu J., Hall P. B., Rafiee A., Schneider D. P., Wu J., 2013, *MNRAS*, **429**, 1479
- Lupton R., Gunn J. E., Ivezić Z., Knapp G. R., Kent S., 2001, in F. R. Harnden Jr., F. A. Primini, & H. E. Payne ed., *Astronomical Society of the Pacific Conference Series Vol. 238, Astronomical Data Analysis Software and Systems X*. p. 269 ([arXiv:astro-ph/0101420](https://arxiv.org/abs/astro-ph/0101420))
- MacLeod C. L., et al., 2010, *ApJ*, **721**, 1014
- MacLeod C. L., et al., 2012, *ApJ*, **753**, 106
- MacLeod C. L., et al., 2015, *ApJ*, **806**, 258
- Magnier E. A., et al., 2013, *ApJS*, **205**, 20
- Margala D., Kirkby D., Dawson K., Bailey S., Blanton M., Schneider D. P., 2015, preprint, ([arXiv:1506.04790](https://arxiv.org/abs/1506.04790))
- Martocchia A., Matt G., Karas V., 2002, *A&A*, **383**, L23
- Merloni A., et al., 2015, *MNRAS*, **452**, 69
- Metcalfe N., et al., 2013, *MNRAS*, **435**, 1825
- Meusinger H., Hinze A., de Hoon A., 2011, *A&A*, **525**, A37
- Morgan C. W., Kochanek C. S., Dai X., Morgan N. D., Falco E. E., 2008, *ApJ*, **689**, 755
- Morganson E., et al., 2014, *ApJ*, **784**, 92
- Morganson E., et al., 2015, *ApJ*, **806**, 244
- Mosquera A. M., Kochanek C. S., Chen B., Dai X., Blackburne J. A., Chartas G., 2013, *ApJ*, **769**, 53
- Myers A. D., et al., 2015, preprint, ([arXiv:1508.04472](https://arxiv.org/abs/1508.04472))
- Nenkova M., Sirocky M. M., Ivezić Ž., Elitzur M., 2008a, *ApJ*, **685**, 147
- Nenkova M., Sirocky M. M., Nikutta R., Ivezić Ž., Elitzur M., 2008b, *ApJ*, **685**, 160
- O'Brien P. T., Goad M. R., Gondhalekar P. M., 1995, *MNRAS*, **275**, 1125

- Osterbrock D. E., 1981, *ApJ*, **249**, 462
 Padmanabhan N., et al., 2008, *ApJ*, **674**, 1217
 Palanque-Delabrouille N., et al., 2013, *A&A*, **551**, A29
 Penston M. V., Perez E., 1984, *MNRAS*, **211**, 33P
 Peterson B. M., 1993, *PASP*, **105**, 247
 Peterson B. M., 2006, in Alloin D., ed., *Lecture Notes in Physics*, Berlin Springer Verlag Vol. 693, *Physics of Active Galactic Nuclei at all Scales*. p. 77, doi:10.1007/3-540-34621-X_3
 Peterson B. M., 2014, *Space Sci. Rev.*, **183**, 253
 Pier J. R., Munn J. A., Hindsley R. B., Hennessy G. S., Kent S. M., Lupton R. H., Ivezić Ž., 2003, *AJ*, **125**, 1559
 Richards G. T., et al., 2002, *AJ*, **123**, 2945
 Richards G. T., et al., 2011, *AJ*, **141**, 167
 Risaliti G., et al., 2009, *ApJ*, **696**, 160
 Rosen S. R., et al., 2015, preprint, ([arXiv:1504.07051](https://arxiv.org/abs/1504.07051))
 Ruan J. J., et al., 2012, *ApJ*, **760**, 51
 Ruan J. J., Anderson S. F., Dexter J., Agol E., 2014, *ApJ*, **783**, 105
 Ruan J. J., et al., 2015, preprint, ([arXiv:1509.03634](https://arxiv.org/abs/1509.03634))
 Runnoe J. C., et al., 2015, preprint, ([arXiv:1509.03640](https://arxiv.org/abs/1509.03640))
 Schmidt K. B., Marshall P. J., Rix H.-W., Jester S., Hennawi J. F., Dobler G., 2010, *ApJ*, **714**, 1194
 Schmidt K. B., Rix H.-W., Shields J. C., Knecht M., Hogg D. W., Maoz D., Bovy J., 2012, *ApJ*, **744**, 147
 Schneider D. P., et al., 2010, *AJ*, **139**, 2360
 Seaton M. J., 1979, *MNRAS*, **187**, 73P
 Sergeev S. G., Doroshenko V. T., Golubinskiy Y. V., Merkulova N. I., Sergeeva E. A., 2005, *ApJ*, **622**, 129
 Sesar B., et al., 2007, *AJ*, **134**, 2236
 Shakura N. I., Sunyaev R. A., 1973, *A&A*, **24**, 337
 Shappee B. J., et al., 2014, *ApJ*, **788**, 48
 Shen Y., et al., 2011, *ApJS*, **194**, 45
 Shen Y., et al., 2015, *ApJS*, **216**, 4
 Simm T., Salvato M., Saglia R., Ponti G., Lanzuisi G., Nandra K., Bender R., 2015, preprint, ([arXiv:1510.06737](https://arxiv.org/abs/1510.06737))
 Smee S. A., et al., 2013, *AJ*, **146**, 32
 Smith J. A., et al., 2002, *AJ*, **123**, 2121
 Stoughton C., et al., 2002, *AJ*, **123**, 485
 Strateva I. V., Brandt W. N., Eracleous M., Schneider D. P., Chartas G., 2006, *ApJ*, **651**, 749
 Stubbs C. W., et al., 2010, *ApJS*, **191**, 376
 Tohline J. E., Osterbrock D. E., 1976, *ApJ*, **210**, L117
 Tonry J. L., et al., 2012, *ApJ*, **750**, 99
 Tran H. D., Osterbrock D. E., Martel A., 1992, *AJ*, **104**, 2072
 Tucker D. L., et al., 2006, *Astronomische Nachrichten*, **327**, 821
 Vanden Berk D. E., et al., 2004, *ApJ*, **601**, 692
 Wilhite B. C., Vanden Berk D. E., Kron R. G., Schneider D. P., Pereyra N., Brunner R. J., Richards G. T., Brinkmann J. V., 2005, *ApJ*, **633**, 638
 York D. G., et al., 2000, *AJ*, **120**, 1579

APPENDIX A: NOTES ON INDIVIDUAL OBJECTS

A list of physical properties for the final sample is provided in Table A1. The luminosities, black hole masses, and Eddington ratios listed are the original SDSS DR7 measurements from Shen et al. (2011). We adopt these values when calculating R_{BLR} and the viscous timescale t_{inft} , since the original luminosity will determine the timescale for subsequent dimming or recovery. However, for the crossing timescales, we adopt the luminosity at 5100Å in the bright state, since this luminosity is presumed to be the intrinsic value in an obscuration scenario. Therefore, for the four quasars in Figure 4 that have “turned on”, the DR7 L_{5100}

values are multiplied by factors of 1.3–1.8 as appropriate when determining t_{cross} .

A1 SDSS J002311.06+003517.5

SN_GAL1 target in BOSS spectroscopy, indicating this object was associated with obtaining the spectrum of host galaxies of SDSS-II supernovae (Dawson et al. 2013). This object is in the Supplementary List of the SDSS-III BOSS DR12 Quasar catalog (DR12Q; Pâris et al. 2016, in advanced prep.) with $z = 0.422$.

A2 SDSS J015957.64+003310.4

TEMPLATE_QSO_SDSS1 target flag in BOSS. This object is not in DR12Q since it is flagged as a “Starforming galaxy” by the BOSS 1-D spectral classification pipeline.

A3 SDSS J022556.07+003026.7

TEMPLATE_GAL_PHOTO target flag in BOSS. This object is in the DR12Q Supplementary list with $z = 0.504$.

Its S82 light curve and multiple BOSS spectra show a 1.5 magnitude dimming over 4.5 yr (rest-frame), during which $H\beta$ vanishes and Mg II strongly diminishes, and then a rebrightening during which the broad components of the Balmer lines (re)appear within 0.7 yr in the rest frame. When measuring the Mg II EW, we estimate the local continuum flux $f_{0,\lambda}(\lambda)$ by subtracting a Gaussian fit to the Mg II line from the observed flux $f_{\lambda}(\lambda)$ and integrating the quantity $(1 - [f_{\lambda}(\lambda)/f_{0,\lambda}(\lambda)])$ over the line.

We find a constant Mg II EW over the 1.5 magnitude dimming from MJD=52944 to 55445, indicating a linear response to the change in flux and a negligible Baldwin effect. What is typically observed for an individual object (with lower-amplitude variability) is an unresponsive Mg II line (e.g., Cackett et al. 2015), so our results suggest that the source of ionizing photons had significantly diminished during this period.

We find from our test in (Section 5.3.1) that extinction by dust can easily explain the large change in the continuum flux and Mg II line, but not the change in $H\beta$. Compared to the observed faint-state spectrum, there is an excess of $H\beta$ flux in the predicted extinguished spectrum at marginal significance ($\sim 1\sigma$ per spectral pixel). Furthermore, the predicted dust crossing timescale for J0225+0030 is about four times too long to explain the dimming in the light curve and ~ 10 times too long to explain the subsequent rebrightening.

A4 SDSS J022652.24-003916.5

QSO_VAR_LF target flag in BOSS indicating this object was specifically targeted due to its variable nature of quasar luminosity function studies (Palanque-Delabrouille et al. 2013). This object is in DR12Q. The relatively small black hole mass for this object yields a viscous timescale t_{inft} that is most similar to the observed optical dimming timescale of several years, but is still an order of magnitude too long (see Table A1).

Table A1. Properties of changing-look quasars, along with estimates for viscous timescale, t_{infl} , and crossing timescales for a BLR cloud and for dust ($t_{\text{cross,BLR cloud}}$ and $t_{\text{cross,dust}}$, respectively). Masses, luminosities, and Eddington ratios are taken from Shen et al. (2011).

Name (SDSSJ)	$\log M_{\text{BH}}/M_{\odot}$	$\log L_{5100}$ [erg s $^{-1}$]	$\log L/L_{\text{Edd}}$	$R_{\text{BLR}}/R_{\text{S}}$	t_{infl} (yr)	$t_{\text{cross,BLR cloud}}$ (days)	$t_{\text{cross,dust}}$ (yr)
002311.06+003517.5	9.23	44.51	-1.85	329	4.4E+06	67.6	19.3
015957.64+003310.4	8.40	44.21	-1.32	1532	5.8E+04	76.5	21.9
022556.07+003026.7	8.35	44.38	-1.10	2112	1.9E+04	108.9	31.1
022652.24-003916.5	7.48	44.34	-0.27	14971	5.6E+01	275.4	78.7
100220.17+450927.3	8.96	44.45	-1.64	569	9.1E+05	61.1	17.5
102152.34+464515.6	8.33	44.15	-1.31	1664	4.8E+04	74.9	21.4
132457.29+480241.2	8.51	44.34	-1.30	1394	6.9E+04	83.9	24.0
214613.31+000930.8	8.94	44.25	-1.82	464	2.0E+06	52.9	15.1
225240.37+010958.7	8.88	44.35	-1.66	602	8.4E+05	85.7	24.5
233317.38-002303.4	10.15	44.31	-2.97	30	6.6E+09	15.6	4.5

A5 SDSS J100220.17+450927.3

J100220.17+450927.3 was selected as being a QSO_CAP and a ROSAT_B, ROSAT_D and ROSAT_E target in SDSS (Richards et al. 2002), and then was selected to be observed in SDSS-III BOSS via the SEQUELS_TARGET and TDSS_FES_DE target flags (Pâris et al. 2016, in advanced prep.; Myers et al. 2015).

SEQUELS is the Sloan Extended QUasar, ELG and LRG Survey, undertaken as part of SDSS-III in order to prepare and refine target selection for the SDSS-IV extended Baryon Oscillation Spectroscopic Survey (eBOSS; Dawson et al. 2015). Another part of SDSS-IV is the Time Domain Spectroscopic Survey (TDSS; Morganson et al. 2015) and the TDSS_FES_DE flag is set for quasar disk emitters selected to be observed by TDSS. These targets are quasars with $i < 18.9$ and broad, double-peaked or asymmetric Balmer emission line profiles, such as those in Strateva et al. (2006, $z < 0.33$ for H α and H β) and higher-redshift analogs from Luo et al. (2013, $z \sim 0.6$ for H β and Mg II). This object appears in DR12Q. For a description of the SDSS-III SEQUELS target flags, see Alam et al. (2015).

A6 J102152.34+464515.6

J1021 was selected via the QSO_CAP target flag in SDSS, and then via SEQUELS_TARGET and TDSS_FES_NQHISN in BOSS. The TDSS_FES_NQHISN target flag is set for $z < 0.8$ DR7 quasars with high signal-to-noise spectra to study broad-line variability on multi-year timescales (Alam et al. 2015).

A7 SDSS J132457.29+480241.2

SEQUELS_TARGET and TDSS_FES_NQHISN target in BOSS. It is not in the DR12Q because of the missing red spectrum.

A8 SDSS J214613.31+000930.8

SN_GAL1 target flag in BOSS. This object is in the DR12Q Supplementary list with $z = 0.622$.

A9 SDSS J225240.37+010958.7

SN_GAL1 target flag in BOSS. This object is in the DR12Q Supplementary list with $z = 0.533$.

A10 SDSS J233317.38-002303.4

SN_GAL1 target flag in BOSS. This object is not in DR12Q.

This paper has been typeset from a $\text{\TeX}/\text{\LaTeX}$ file prepared by the author.